

# RD-Optimized Trit-Plane Coding of Deep Compressed Image Latent Tensors

Seungmin Jeon  
Korea University

seungminjeon@mcl.korea.ac.kr

Jae-Han Lee  
Korea University

jaehanlee@mcl.korea.ac.kr

Chang-Su Kim  
Korea University

changasukim@korea.ac.kr

## Abstract

*DPICT is the first learning-based image codec supporting fine granular scalability. In this paper, we describe how to implement two key components of DPICT efficiently: trit-plane slicing and RD-prioritized transmission. In DPICT, we transform an image into a latent tensor, represent the tensor in ternary digits (trits), and encode the trits in the decreasing order of significance. For entropy encoding, we should compute the probability of each trit, which demands high time complexity in both the encoder and the decoder. To reduce the complexity, we develop a parallel computing scheme for the probabilities and describe it in detail with pseudo-codes. Moreover, in this paper, we compare the trit-plane slicing in DPICT with the alternative bit-plane slicing. Experimental results show that the time complexity is reduced significantly by the parallel computing and that the trit-plane slicing provides better rate-distortion performances than the bit-plane slicing.*

## 1. Introduction

Image compression is an important topic in the field of image processing. There are classical codecs, such as JPEG [1], JPEG2000 [2] and BPG [6]. They have been developed to achieve efficient data compression and transmission. These classical codecs rely on the separately designed hand-crafted modules, so they are not optimal as a entire structure.

Recently, with the great success of deep learning in various fields of image processing, deep learning has been adopted for image compression, as well as other fields of image processing. Among these learning-based codecs, CNN-based ones [4, 5, 7, 14] show competitive performance in terms of rate-distortion compared to classical codecs. They transform the input image to latent representation using encoder and compress it to a bitstream. Latent representation is reversely transformed to the reconstructed image by decoder. Ballé *et al.* [4, 5] proposed an additive uniform noise for the backpropagation problem in the training phase and additional autoencoder for hyperprior. Minnen

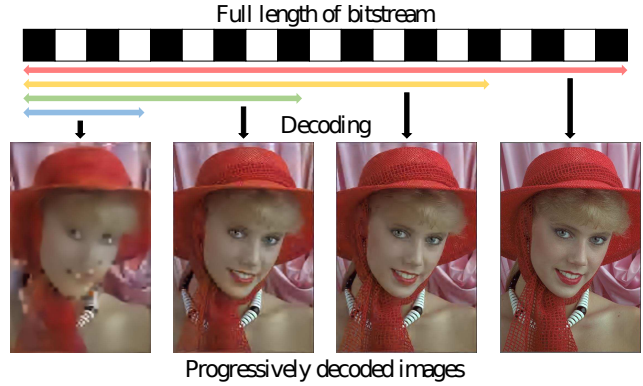


Figure 1. Illustration of progressive image coding.

*et al.* [14] adopts context model to estimate entropy parameters of latent representation. Cheng *et al.* [7] assumed Gaussian mixture models for latent representation. However, these codecs only support fixed-rate compression, so for various compression of  $N$  rates, they train the network for  $N$  times.

Progressive compression, or scalable coding [15] is an important task in the field of data compression. Here, progressive compression means the algorithm that encodes a data into a single bitstream and this bitstream can be reconstructed to various qualities of data which have different bitrates, as shown in fig1. It is a lot of uses for the progressive coding. There are many display devices in these days, and each of them has a different resolution. A single progressive bitstream can be decoded into various resolution images of the same information. It is efficient more than non-progressive one. Classical codecs like JPEG and JPEG2000 support progressive compression and there are also learning-based codecs [9, 11, 16, 17]. Most of the learning-based codecs are based on recurrent neural networks(RNNs). Toderici *et al.* [16] proposed the first RNN-based progressive compression network. Their network transmit bitstream progressively using long short-term memory(LSTM). Gregor *et at.* [9] introduced a recurrent image codec, which improves conceptual quality using a generative model. However, these codecs [9, 16] are for

low-resolution patches only. Toderici *et al.* [17] developed a codec for higher-resolution images by expanding the previous work in [16]. Johnston *et al.* [11] proposed an effective initializer for hidden states of their RNN and a spatially adaptive rate controller. However, the performances of these RNN-based codecs are inferior even to those of the traditional codecs [6].

We analyze algorithms of the previous work, DPIC: Deep progressive image compression using trit-planes [13]. We also analyze the progressive compression algorithm bit-plane slicing additionally. First, by showing the distribution and visualization of latent representations, we demonstrate that trit-plane slicing can reconstruct the values of latent representation better than bit-plane slicing. In latent representation, there are considerable numbers of elements which have values close to zero. The trit-plane slicing estimates the zero-closed values to zero in the intermediate reconstruction of low rates. The bit-plane slicing shows better RD performance compared to trit-plane slicing in high rates. It is because the bit-plane slicing has more number of planes so it can reconstruct the latent representation more finer. We also describe the implementation of DPIC in python. We presents how to implement the trit-plane slicing and sorting elements by RD priorities. In this process of using probability mass functions of elements, we use parallel computing instead of iterations to reduce the time cost.

## 2. PROPOSED ALGORITHM

In this section, we analyze the bit-plane and trit-plane slicing algorithms. For the explanation of algorithms, we use some notations. As plotted in fig 2,  $\mathbf{X}$  is an RGB input image and  $\mathbf{Y} \in \mathbb{R}^{C \times H \times W}$  denote a latent representation tensor transformed by the encoder, respectively.  $\mathbf{M}, \Sigma \in \mathbb{R}^{C \times H \times W}$  denote a mean and a standard deviation of  $\mathbf{Y}$ , respectively.  $\mathbf{Y}_c$  and  $\hat{\mathbf{Y}}_c$  denote the zero-centered  $\mathbf{Y}$  and quantization of  $\mathbf{Y}_c$ , respectively. In other words,  $\hat{\mathbf{Y}}_c = q(\mathbf{Y}_c) = q(\mathbf{Y} - \mathbf{M})$ . Rounding function is used for quantization.  $\hat{\mathbf{Y}}_c$  is the one encoded into bitstream. We use the same network structure as used in previous work [7], but we eliminate autoregressive model used to estimate entropy parameters [14] and gaussian mixture model [7]. Because of the progressive reconstructions of  $\hat{\mathbf{Y}}_c$ , autoregressive model cannot estimate entropy parameters consistently.

### 2.1. Bit and Trit-Plane Slicing

#### 2.1.1 Bit-plane slicing

$\hat{\mathbf{Y}}_c$  can be represented in a binary number system and it can be encoded using bit-plane slicing. First, let  $y_i$  and  $\sigma_i$  the  $i$ th element of  $\hat{\mathbf{Y}}_c$  and its standard deviation, respectively. Here,  $i$  is an integer,  $0 \leq i \leq (K - 1)$ , and  $K$  is the number of elements in the latent tensor  $\hat{\mathbf{Y}}_c$ . The whole interval  $\mathcal{I}_0$

where  $y_i$  belongs to can be defined by using  $\sigma_i$ .

$$l = \lceil \log_2(2 \cdot \sigma_i \cdot \Phi^{-1}(p_t)) \rceil, \quad (1)$$

$$\mathcal{I}_0 = [l_0, r_0) = [-\frac{2^l-1}{2}, \frac{2^l-1}{2}) \quad (2)$$

where  $\Phi(\cdot)$  denotes the cumulative density function(CDF) of the standard normal distribution and  $p_t$  a probability with tiny value.  $(1 - 0.5 \times 10^{-9})$  is used for  $p_t$  in this work and then the value of  $l$  is around 6.11. The whole interval  $\mathcal{I}_0$  means the smallest interval with value of powers of 2 where the integral sum of distribution is larger than  $(1 - 1 \times 10^{-9})$ . We divide  $\mathcal{I}_0$  by 2 with the same length. Let  $b_0$  the first bit of  $y_i$ . If  $y_i < \frac{l_0+r_0}{2}$ ,  $b_0 = 0_{(2)}$ . If  $y_i \geq \frac{l_0+r_0}{2}$ , then  $b_0 = 1_{(2)}$ . And the same process is repeated sequentially.

In more generalized expression, let  $\mathcal{I}_n = [l_n, r_n)$  the interval when the first  $n$ th planes are encoded.  $y_i$  must be in  $\mathcal{I}_0$ . And let  $b_n \in \{0_{(2)}, 1_{(2)}\}$  denotes the  $n$ th bit of  $y_i$ . Similar to the example above,  $\mathcal{I}_0$  is divided by 2 subintervals,

$$\mathcal{I}_n^0 = [l_n^0, r_n^0) = [l_n, \frac{l_n+r_n}{2}), \quad (3)$$

$$\mathcal{I}_n^1 = [l_n^1, r_n^1) = [\frac{l_n+r_n}{2}, r_n). \quad (4)$$

Then, the next  $(n + 1)$ th bit  $b_{n+1}$  is determined by which subinterval the  $y_i$  belongs to. The selected subinterval then becomes  $\mathcal{I}_{n+1}$ . The  $n$ th bits of the whole elements form the  $n$ th bit-plane and the arithmetic encoder compress these bit-planes sequentially in order from the first plane to the last plane. For arithmetic coding, the coder needs conditional probability mass function(PMF) of  $b_n$  given  $\{b_{n-1}, \dots, b_1\}$ ,

$$P(b_n = k | b_{n-1}, \dots, b_1) = P(y_i \in \mathcal{I}_n^k | y_i \in \mathcal{I}_{n-1}) \quad (5)$$

$$= \frac{\Phi(r_n^k/\sigma_i) - \Phi(l_n^k/\sigma_i)}{\Phi(r_{n-1}/\sigma_i) - \Phi(l_{n-1}/\sigma_i)} \quad (6)$$

where  $k \in \{0_{(2)}, 1_{(2)}\}$ .

In the decoding phase, the network transformed partially decoded bit-planes to the reconstructed latent representation  $\hat{y}_i^n$ . Given the sequence of sliced bits  $\{b_n, b_{n-1}, \dots, b_1\}$ , the reconstructed  $\hat{y}_i^n$  is estimated by the expectation of  $y_i$  given  $y_i \in \mathcal{I}_n$

$$\hat{y}_i^n = E_{y_i \sim p_{y_i}} [y_i | y_i \in \mathcal{I}_n] \quad (7)$$

which minimizes the mean square error(MSE) between  $y_i$  and  $\hat{y}_i^n$ .

#### 2.1.2 Trit-plane slicing

As described in Section 2.1.1, the trit-plane slicing carries out similar processes but the division of intervals are different. First, equation (2) are modified in the trit-plane slicing, such as

$$\mathcal{I}_0 = [l_0, r_0) = [-\frac{3^l-1}{2}, \frac{3^l-1}{2}). \quad (8)$$

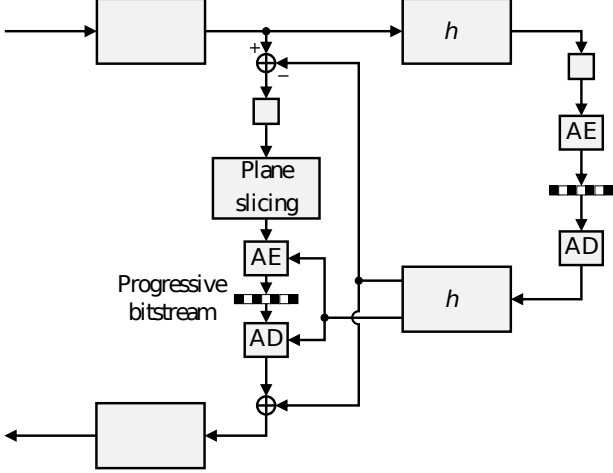


Figure 2. Framework of the network used in this work. AE and AD means an arithmetic encoder and decoder, respectively.

The way to divide interval is also similar to equation (3) and (4), like

$$\mathcal{I}_n^0 = [l_n^0, r_n^0) = [l_n, \frac{2l_n+r_n}{3}), \quad (9)$$

$$\mathcal{I}_n^1 = [l_n^1, r_n^1) = [\frac{2l_n+r_n}{3}, \frac{l_n+2r_n}{3}), \quad (10)$$

$$\mathcal{I}_n^2 = [l_n^2, r_n^2) = [\frac{l_n+2r_n}{3}, r_n). \quad (11)$$

Let  $t_n \in \{0_{(3)}, 1_{(3)}, 2_{(3)}\}$  denotes the  $n$ th trit of  $y_i$ . Using these divided subintervals, the  $(n+1)$ th trit  $t_{n+1}$  is determined by the same process in Section 2.1.1. Also in trit-plane slicing, the  $n$ th trits form the  $n$ th trit-plane, and these are compressed sequentially by arithmetic coder. The way to reconstruct trits to  $\hat{y}_i^n$  is same with bit-plane slicing.

### 3. Implementation

## 4. Experimental Results

### 4.1. Details

We use the Vimeo90k dataset [19] for training. It contains several frames from overlapping contents, so we sample 80000 frames. We crop training datasets by  $256 \times 256$  randomly. We evaluate the compression performance of the proposed algorithm using Kodak loseless image dataset [3] which consists of 24 images of resolution  $512 \times 768$  or  $768 \times 512$ .

We use the Adam optimizer [12] with a learning rate of  $10^{-4}$ , a batch size of 16 and  $\lambda = 0.2$ . We trained the network for 200 epochs and scheduled the learning rate using cosine annealing cycles [10]. For comparison of progressive algorithm with fixed-rate compression results, we train the network with  $\lambda \in \{0.0125, 0.025, 0.05, 0.1, 0.2\}$  and plot the RD curves in fig 3. We evaluate the network rate performance using bits per pixel(bpp), which means the

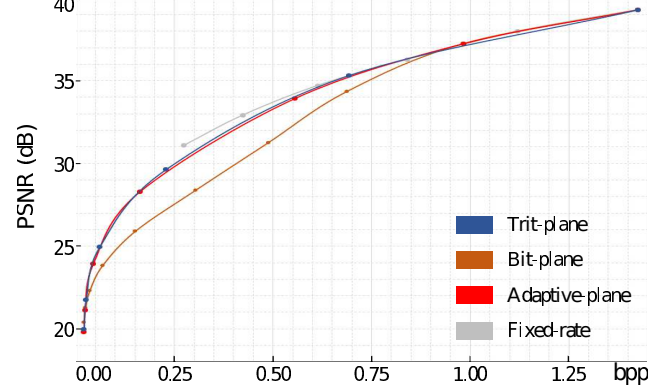


Figure 3. RD performance comparison of the trit-plane, bit-plane adaptive-plane and fixed-rate.

length of binary bitstream divided by the number of pixels of input image  $\mathbf{X}$ . We use the PSNR and MS-SSIM [18] for distortion metrics. For the arithmetic coder, we use rANS coder [8]. When estimating conditional pmfs in (5), the network needs to calculate  $K = C \times H \times W$  numbers of pmf to compress a plane.

### 4.2. Performance assessment

In this section, we focus on the analysis between several plane slicing methods. We compare the trit-plane slicing algorithm with the bit-plane slicing and adaptive-plane slicing. When we implemented adaptive-plane slicing, we use 2 for  $n$  which is mentioned in Section ??.

Fig 3 plots the RD curves on the Kodak datasets. The networks are trained using mse distortion loss. At low rates under around 0.9bpp, bit-plane coding shows worse than the other methods, but in high rates, it surpasses the performance of trit-plane. It shows that using plenty of planes, the bit-plane slicing reconstruct  $\hat{\mathbf{Y}}_c$  more finer than the trit-plane slicing. In other words, the adaptive-plane slicing divide the interval into 3 in low rates and into 2 in high rates, so the curve is close to the curve of trit-plane slicing in low rates, and it also surpasses the trit-plane slicing in high rates.

Fig 4 shows the qualitative results reconstructed by each slicing method at similar rates. Compared to bit-plane, trit-plane reconstruct image details in specific textures and boundaries between different regions, for example, region around the letters or the boundary of sky and a house, more accurately. Adaptive-plane shows comparable reconstructions compared to trit-plane.

There is the distribution of  $\hat{\mathbf{Y}}_c$  of the average of whole images in Kodak dataset in fig 5. As shown in fig 5, the frequency of values around zero accounts for the most, and it has a distribution close to gaussian. The trit-plane slicing preserves more zeros in the earlier reconstruction of  $\hat{\mathbf{Y}}_c$  than the others, because it reconstruct the sequence of



Figure 4. Qualitative comparison of reconstructed images  $\hat{X}$  of trit-plane, bit-plane, adaptive-plane at similar bpps.

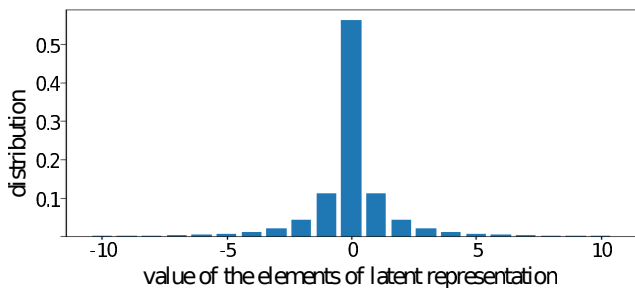


Figure 5. The average distribution of  $\hat{Y}_c$  for Kodak dataset.

$\{1_{(3)}, \dots\}$  for 0 but the bit-plane slicing does not. So, the bit-plane slicing shows worse performance compared to the others.

Fig 6 shows the visualization of latent representations of the channel which has the highest entropy using one of the image in the Kodak dataset. In column 2 and 3 of fig 6, the intermediate reconstructions of  $\hat{Y}_c$  of bit-plane slicing and trit-plane slicing and their error maps are visualized respectively. To highlight the values near 0, the visualizations of latents  $\hat{Y}_c$ ,  $\hat{Y}_{c,bit}^n$ ,  $\hat{Y}_{c,trit}^n$  are truncated by  $[-40, 40]$ . Comparing the latent images in column 2, trit-plane slicing has more values near 0 than bit-plane slicing, and the visualization of trit-plane slicing is more close to the one of original latent representation. Because the trit-plane slicing reconstructs the values around zero of  $\hat{Y}_c$  more precisely, the trit-plane slicing has lower error than the bit-plane slicing, as shown in the white pixels in the figures in column 3.

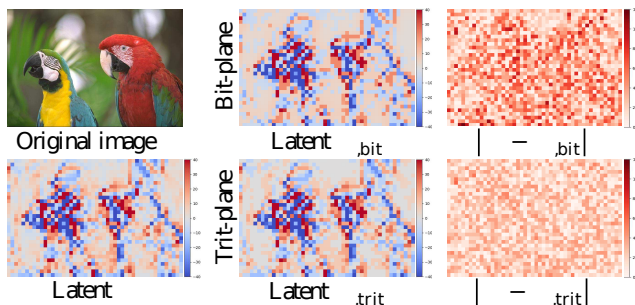


Figure 6. Visualization of latent representations of input image, trit-plane and bit-plane using “kodim23”.

## 5. Conclusions

We analyzed the bit-plane slicing and the previous work [13], and proposed an progressive coding algorithm using adaptive-plane slicing. In the network, a latent representation is obtained from an input image. For the same latent representation, the rate-distortion curves of progressive coding vary depending on how to slice the latent. We show that the distribution of quantized latent which centered to zero affects the aspect of performance. Experimental results show that the trit-plane slicing and the adaptive-plane slicing provides better performance for progressive coding significantly.

## References

- [1] *The Independent JPEG Group’s JPEG software.*

- <https://ijg.org>. 1
- [2] *JPEG2000 official software OpenJPEG*. <https://jpeg.org/jpeg2000/software.html>. 1
- [3] *Kodak Lossless True Color Image Suite*. [Online]. Available: <http://r0k.us/graphics/kodak>. 3
- [4] Johannes Ballé, Valero Laparra, and Eero P. Simoncelli. End-to-end optimized image compression. In *ICLR*, 2017. 1
- [5] Johannes Ballé, David Minnen, Saurabh Singh, Sung Jin Hwang, and Nick Johnston. Variational image compression with a scale hyperprior. In *ICLR*, 2018. 1
- [6] Fabrice Bellard. *BPG Image format*. 2014. <https://bellard.org/bpg>, Retrieved 2016-04-02. 1, 2
- [7] Zhengxue Cheng, Heming Sun, Masaru Takeuchi, and Jiro Katto. Learned image compression with discretized gaussian mixture likelihoods and attention modules. In *CVPR*, pages 7939–7948, 2020. 1, 2
- [8] Jarek Duda. Asymmetric numeral systems: entropy coding combining speed of Huffman coding with compression rate of arithmetic coding. *arXiv preprint arXiv:1311.2540*, 2013. 3
- [9] Karol Gregor, Frederic Besse, Danilo Jimenez Rezende, Ivo Danihelka, and Daan Wierstra. Towards conceptual compression. *NeurIPS*, 29:3549–3557, 2016. 1
- [10] Gao Huang, Yixuan Li, Geoff Pleiss, Zhuang Liu, John E. Hopcroft, and Kilian Q. Weinberger. Snapshot ensembles: Train 1, get m for free. In *ICLR*, 2017. 3
- [11] Nick Johnston, Damien Vincent, David Minnen, Michele Covell, Saurabh Singh, Troy Chinen, Sung Jin Hwang, Joel Shor, and George Toderici. Improved lossy image compression with priming and spatially adaptive bit rates for recurrent networks. In *CVPR*, pages 4385–4393, 2018. 1, 2
- [12] Diederik P. Kingma and Jimmy Ba. Adam: A method for stochastic optimization. In *ICLR*, 2015. 3
- [13] Jae-Han Lee, Seungmin Jeon, Kwang Pyo Choi, Youngo Park, and Chang-su Kim. DPICT: Deep progressive image compression using trit-planes. *arXiv preprint arXiv:2112.06334*, 2021. 2, 4
- [14] David Minnen, Johannes Ballé, and George Toderici. Joint autoregressive and hierarchical priors for learned image compression. In *NeurIPS*, 2018. 1, 2
- [15] J.-R. Ohm. Advances in scalable video coding. *Proc. IEEE*, 93(1):42–56, 2005. 1
- [16] George Toderici, Sean M O’Malley, Sung Jin Hwang, Damien Vincent, David Minnen, Shumeet Baluja, Michele Covell, and Rahul Sukthankar. Variable rate image compression with recurrent neural networks. In *ICLR*, 2016. 1, 2
- [17] George Toderici, Damien Vincent, Nick Johnston, Sung Jin Hwang, David Minnen, Joel Shor, and Michele Covell. Full resolution image compression with recurrent neural networks. In *CVPR*, pages 5306–5314, 2017. 1, 2
- [18] Zhou Wang, Eero P. Simoncelli, and Alan C. Bovik. Multiscale structural similarity for image quality assessment. In *The Thirty-Seventh Asilomar Conference on Signals, Systems & Computers, 2003*, volume 2, pages 1398–1402, 2003. 3
- [19] Tianfan Xue, Baian Chen, Jiajun Wu, Donglai Wei, and William T. Freeman. Video enhancement with task-oriented flow. *IJCV*, 127(8):1106–1125, 2019. 3